THE ASTROPHYSICAL JOURNAL, 442:662–667, 1995 April 1

NEAR- AND FAR-INFRARED OBSERVATIONS OF INTERPLANETARY DUST BANDS FROM THE *COBE*[1] DIFFUSE INFRARED BACKGROUND EXPERIMENT

WILLIAM J. SPIESMAN,[2,3] MICHAEL G. HAUSER,[4] THOMAS KELSALL,[5] CAREY M. LISSE,[6]
S. HARVEY MOSELEY, JR.,[5] WILLIAM T. REACH,[7] ROBERT F. SILVERBERG,[5]
SALLY W. STEMWEDEL,[8] AND JANET L. WEILAND[9]
Received 1994 May 17; accepted 1994 October 10

ABSTRACT

Data from the Diffuse Infrared Background Experiment (DIRBE) instrument aboard the *COBE* spacecraft have been used to examine the near and far infrared signatures of the interplanetary dust (IPD) bands. Images of the dust band pairs at ecliptic latitudes of $\pm 1\overset{\circ}{.}4$ and $\pm 10°$ have been produced at DIRBE wavelengths from 1.25 to 100 μm. The observations at the shorter wavelengths provide the first evidence of scattered sunlight from particles responsible for the dust bands. It is found that the grains in the bands and those in the smooth IPD cloud have similar spectral energy distributions, suggesting similar compositions and possibly a common origin. The scattering albedos from 1.25 to 3.5 μm for the grains in the dust bands and those in the smooth IPD cloud are 0.22 and 0.29, respectively. The 10° band pair is cooler (185 ± 10 K) than the smooth interplanetary dust cloud (259 ± 10 K). From both parallactic and thermal analyses, the implied location of the grains responsible for the peak brightness of the 10° band pair is 2.1 ± 0.1 AU from the Sun. A parallactic distance of 1.4 ± 0.2 AU is found for the peak of the $1\overset{\circ}{.}4$ band pair.

Subject headings: infrared: solar system — interplanetary medium

1. INTRODUCTION

The interplanetary dust (IPD) bands were discovered by Low et al. (1984) in the 12 to 100 μm data from the Infrared Astronomical Satellite (*IRAS*). They are seen as small "shoulders" on the broad thermal emission concentrated toward the ecliptic plane. The emission from the dust bands represents an enhancement of only a few percent above the smooth component of IPD emission described by Hauser et al. (1984). The bands come in pairs, symmetrically distributed about the ecliptic plane. At angular resolution of $\frac{1}{2}°$, the brightest of these pairs are located at approximately $\pm 1\overset{\circ}{.}4$ and $\pm 10°$ geocentric ecliptic latitude. *IRAS* data also show a third band pair at $\pm 17°$ and suggest other bands at $\pm 24°$ (Sykes 1988; Reach 1991a).

The bands are believed to arise from dust in common inclination orbits, and the inclinations have been linked with asteroid families found near 3 AU (Dermott et al. 1984; Low et al. 1984; Sykes 1990). Sykes & Greenberg (1986) developed a model for the origin of the dust bands in the collisional disruption of a small (~15 km) asteroid. The debris are distributed over the orbit of a progenitor asteroid and then spread into an edge-brightened torus due to differential precession by Jupiter. Sykes (1990) compared the predicted latitudes of band pairs associated with the major asteroid families with the locations of features in the enhanced *IRAS* data (Sykes 1988), finding strong evidence for bands associated with the Koronis and Themis families, and possible evidence for bands associated with other families such as the Eos and Maria families. At $\frac{1}{2}°$ resolution, the Koronis and Themis bands are blended into the band pair at $\pm 1\overset{\circ}{.}4$. Reach (1991b) has suggested that the inner edge of the dust bands extends inside the Earth's orbit, because Poynting-Robertson drag causes the semi-major axis of particle orbits to decay on time scales shorter than the time required for band-pair formation.

The DIRBE is a powerful instrument for the study of the IPD. It redundantly surveys the sky for solar elongation angles from 64° to 124°, and it does so not only at the wavelengths of the *IRAS* survey and longer, but at 1.25, 2.2, 3.5, and 4.9 μm. This allows the confirmation of *IRAS* observations, a search for time dependence over the seven years between the *IRAS* and *COBE* missions, a determination of the apparent location of the dust band material responsible for the peak brightness by color temperature and parallax, and a particle albedo determination for IPD features that are detected in scattered light. Polarization measurements with the DIRBE also reveal characteristics of the IPD grains (Berriman et al. 1994), but in this paper we consider only the photometric measurements.

2. OBSERVATIONS

The Diffuse Infrared Background Experiment (DIRBE) was launched 1989 November 18 on board the *Cosmic Background Explorer* (*COBE*). The DIRBE instrument is described in detail elsewhere (Hauser et al. 1991; Boggess et al. 1992; Silverberg et al. 1993), but the basic instrument characteristics are shown in Table 1.

[1] The National Aeronautics and Space Administration/Goddard Space Flight Center (NASA/GSFC) is responsible for the design, development, and operation of the *Cosmic Background Explorer* (*COBE*). Scientific guidance is provided by the *COBE* Science Working Group. GSFC is also responsible for the analysis software and for the production of the mission data sets.

[2] Eureka Scientific, Inc., 2452 Delmer Street, Suite 100, Oakland, CA 94602.
[3] Visiting Astronomer, Astronomy Department, RLM 16.232, University of Texas at Austin, Austin, Texas, 78712; spies@clyde.as.utexas.edu.
[4] NASA Goddard Space Flight Center, Code 680, Laboratory for Astronomy and Solar Physics, Greenbelt, MD 20771.
[5] NASA Goddard Space Flight Center, Code 685, Laboratory for Astronomy and Solar Physics, Greenbelt, MD 20771.
[6] Hughes STX, Code 685.9, NASA Goddard Space Flight Center, Greenbelt, MD 20771.
[7] Universities Space Research Association, Code 685, NASA Goddard Space Flight Center, Greenbelt, MD 20771.
[8] Applied Research Corporation, Code 685.3, NASA Goddard Space Flight Center, Greenbelt, MD 20771.
[9] General Sciences Corporation, Code 685.3, NASA Goddard Space Flight Center, Greenbelt, MD 20771.

TABLE 1

THE DIRBE INSTRUMENT

Parameter	Value
Wavelength coverage (μm)	1.25, 2.2, 3.5, 4.9, 12, 25, 60, 100, 140, 240
Polarization coverage (μm).....	1.25, 2.2, 3.5
Instantaneous field of view.....	0°.7 square, seen simultaneously at all wavelengths
Sky coverage.....	entire sky surveyed highly redundantly
Solar elongation.....	ranges from 64° to 124°

All detectors in the DIRBE view the same instantaneous 0°.7 × 0°.7 field of view. Since the DIRBE's line of sight is inclined at 30° to the spin axis of the *COBE*, it scans the sky with a helical scan pattern as the *COBE* spacecraft spins at 0.8 RPM and the spacecraft orbits the Earth. Each loop of the helix is offset by about $2\frac{1}{2}$ beam widths from the previous one, so the scan pattern from a single orbit leaves holes in sky coverage. These holes are nominally filled in within the 14 orbits of a day. This scan pattern provides hundreds of observations every six months of each direction in the sky as the solar elongation, the angle between the Sun and the line of sight, varies within the range from 64° to 124°.

The DIRBE is an absolute photometer, switching its beam between the sky and an internal zero-flux reference at a rate of 32 Hz. The magnitude and stability of instrumental zero point offsets and photometric responsivity are checked about five times per orbit by closing a full beam shutter, measuring the "dark" signal, and then stimulating the detectors with stable internal reference sources. This provides both zero point calibration and very precise relative photometry on daily time scales. Long-term photometric scale stability is maintained using observations of stable, discrete celestial sources throughout the mission. Short-term and long-term photometric stability obtained in this way is typically better than 1%.

The data presented here are from the period 1990 July 30 to 1990 September 21. Preliminary absolute calibration is based upon observations of a single celestial reference source at each wavelength: Sirius for the range 1.25 to 12 μm, NGC 7027 at 25 μm, Uranus at 60 and 100 μm, and Jupiter at 140 and 240 μm. The estimated absolute systematic calibration error is less than 20% at each wavelength, and relative errors are less than 5% at wavelengths where the calibration is based upon the same reference source.

3. DATA REDUCTION

Extraction of the weak interplanetary dust band signal from data is not a simple task. The *IRAS* data have been analyzed using a variety of different techniques: Dermott et al. (1988) used Fourier decomposition, Sykes (1990) used a median filtering technique, and Reach (1992) used a combination of polynomial and Gaussian fitting. The DIRBE data are of lower angular resolution than the *IRAS* data, further adding to the challenge.

3.1. *Robust Averaging*

In order to enhance the smooth component and bands in the interplanetary dust signal relative to non-IPD contributions, a robust averaging technique which is insensitive to outliers is employed. Weight is given only to those data samples which are minimally impacted by interstellar, stellar and planetary contributions to the total sky brightness. To this end, the DIRBE data for each wavelength have been binned onto an ecliptic latitude, solar elongation (β, ϵ) grid as follows:

1. DIRBE observations are pixelized in geocentric ecliptic coordinates, with each pixel roughly 0°.3 square. Intensity values for each pixel are obtained weekly by averaging good quality observations. This step removes data flagged as noisy (e.g., cosmic ray hits or electronic noise spikes), saturated data values, data taken while *COBE* was in the South Atlantic Anomaly, data taken while pointing too near the Moon, and data contaminated by events on the spacecraft.

2. The data for a series of ~8 consecutive weeks of weekly averaged DIRBE observations are binned in a grid as a function of β and ϵ. On the basis of *IRAS* results we assume that the structure of the bands depends weakly on time and ecliptic longitude, and overlay the images from each week to improve the signal-to-noise level of the bands. The apparent ecliptic latitudes of the dust bands vary approximately sinusoidally over the course of a year, limiting the useful integration time to a few months before the dust band images become smeared out.

3. Within a given (β, ϵ) bin, each datum represents a unique measure of the elongation-dependent interplanetary dust signal plus "contamination" from other celestial sources. Since the celestial sphere moves with respect to this Sun-Earth referenced coordinate system (fixed relative to the Sun-Earth line), celestial sources move through each (β, ϵ) bin. Thus, some measurements of a given bin are perturbed by celestial sources to a greater degree than are others. The small angular scale solar system and extra-solar system contribution to the signal is minimized by assigning zero weights to all but the lowest intensities observed in a given bin. Because individual intensity measurements in a bin are themselves averages over an entire week, this selection process minimally impacts the statistical significance of the measurement for a given bin, while significantly reducing systematic contamination from non-IPD sources.

This selection technique has several advantages over other methods of isolating the interplanetary dust signal in the data. (1) It avoids the difficult business of filtering out unresolved sources in the time domain, which can introduce artifacts into the data. Because of the quasi-synchronous character of the *COBE* orbit exhibited by an almost exact integral number of orbits per day, and by near commensurability of the spacecraft spin and orbital periods, time-domain filtering can produce complicated low signal-level artifacts. (2) It removes the necessity of making model-dependent assumptions about the intrinsic shape of the interplanetary dust signal component. A disadvantage of this method is that the data are averaged over 8 weeks. This tends to smear out variations in the interplanetary dust cloud that occur in less than 60° of Earth travel around the Sun. In effect this reduction method makes a multiply exposed photograph of the dust bands, one exposure each week.

The results of the data-averaging process described above are displayed for wavelengths of 1.25 and 25 μm as surface

plots in Figures 1*a* and 1*b* (Plate 2). The central ridge at the ecliptic equator is easily identified at 25 μm. The 1°.4 and 10° dust bands are seen as secondary ridges to either side of the ecliptic equator. Only the central ridge from the smooth interplanetary dust component is clear in the 1.25 μm image, and further enhancements are necessary to bring out the dust bands.

3.2. *Image Processing*

In order to measure the precise location of the dust bands, which are difficult to identify in the best of circumstances (12 and 25 μm data), image enhancing techniques are used. Unsharp masking yields the best results:

$$B = DATA - SMOOTH(DATA) \quad (1)$$

where "DATA" is the original (β, ϵ)-gridded data set and "SMOOTH" is a square two-dimensional boxcar smoothing function. The resulting image B shows areas where DATA has edges and changes of inflection.

The size of the boxcar window is adjusted to bring out particular features: a 10° wide boxcar enhances the 10° band pair, while a quite narrow 1° boxcar is needed to enhance the 1°.4 band pair, because of its proximity to the peak of the smooth component of IPD emission and the DIRBE instrument's low angular resolution.

4. INTERPLANETARY DUST BAND IMAGES AND ENERGY DISTRIBUTIONS

The image enhancement technique described above works quite well at 12 and 25 μm (Figs. 1*d* and 2 [Plates 2 and 3]). Although the dust bands are by no means obvious in the averaged near-infrared data (Fig. 1*a*), the same technique is applied there. At very low signal-to-noise, the 10° dust bands are seen in scattered light at the same locations as at 12 and 25 μm (Figs. 1*c* and 2). This is verified at the 95% level of certainty by a cross-correlation of the 1.25 and 25 μm images. Note that at 1.25 μm the northern member is particularly evident, its apparent latitude increasing with elongation. At the shorter infrared wavelengths the dust bands are most evident at 1.25 μm, and then weaken toward longer wavelengths, as is expected for scattered solar radiation. The band signal then strengthens at wavelengths longer than 4.9 μm as thermal radiation from the particles increases.

The DIRBE has provided the first observational evidence of the IPD bands in scattered solar light at 1.25, 2.2, 3.5, and 4.9 μm (see Fig. 3). Figure 2 shows the gridded, filtered intensity maps from 1.25 to 100 μm. Because the IPD signal becomes weak in the very far infrared, and the DIRBE is least sensitive at its longest wavelengths, no dust bands were identified at 140 or 240 μm.

The spectral energy distributions for the smooth component of the IPD signal in the ecliptic plane and for the dust band located near +10° ecliptic latitude are derived for the DIRBE observations from 1.25 to 100 μm at 90° solar elongation. Using the robustly averaged data described in § 3.1, the smooth interplanetary dust background is modeled using a six-parameter empirical function formulated by Hauser (1993). This smooth component is then subtracted from the total signal to obtain the dust band contribution. The energy distributions for the dust band and for the smooth IPD component are shown in Figures 3 and 4, respectively. Both

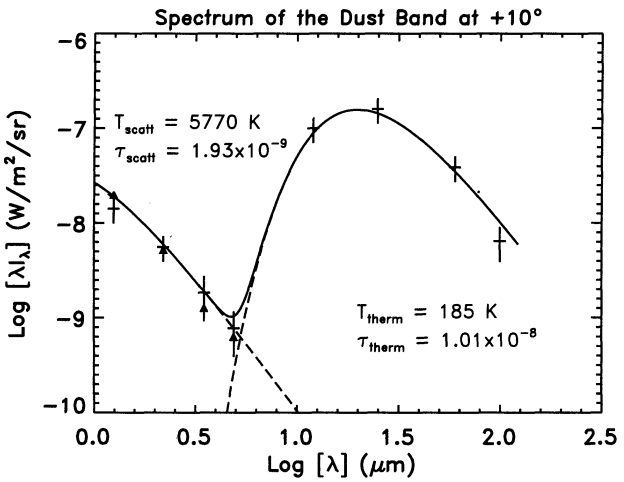

FIG. 3.—Energy distribution for the $\beta = +10°$ dust band at 90° elongation. Dashed curves are graybody fits to the data in the scattering and thermal emission regimes separately. The smooth curve is the sum of the two components. The small triangles show the specific solar intensity at the DIRBE wavelengths.

distributions clearly show contributions from scattering and from thermal emission.

5. INTERPRETATION

5.1. *Parallactic Distance to the Observed Bands*

The apparent ecliptic latitude of the brightest peaks of an observed band pair, as well as the variation in apparent separation of the two brightest peaks with elongation, depend upon the distance of the observer from the material responsible for the brightest regions of the bands and the separation of the bands from each other (Grün et al. 1985; Sykes 1990). Hence, parallactic distances to the brightest features can be determined from the DIRBE maps in the (β, ϵ) grid. Band radii are found by making two or more measurements of the band separation as a function of elongation, thus eliminating the unknown distance between the bands from equation (2) below. In practice, we made measurements at four elongations for each image and calculated an error based on the distribution of the solutions determined using all possible permutations of measurement pairs.

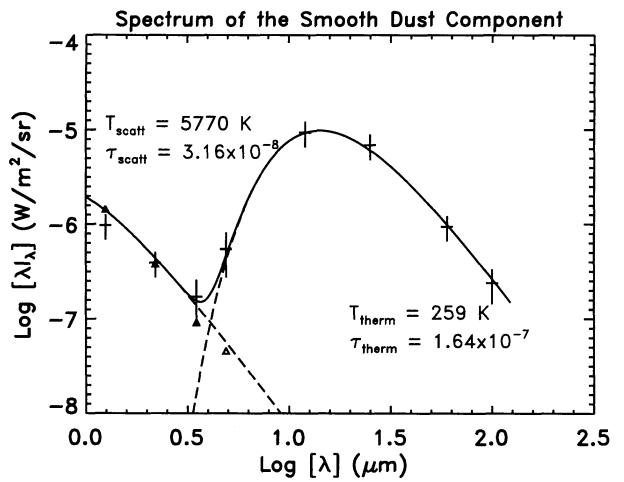

FIG. 4.—Same as Fig. 3, but for the smooth IPD at ecliptic latitude 0° and elongation 90°.

PLATE 2

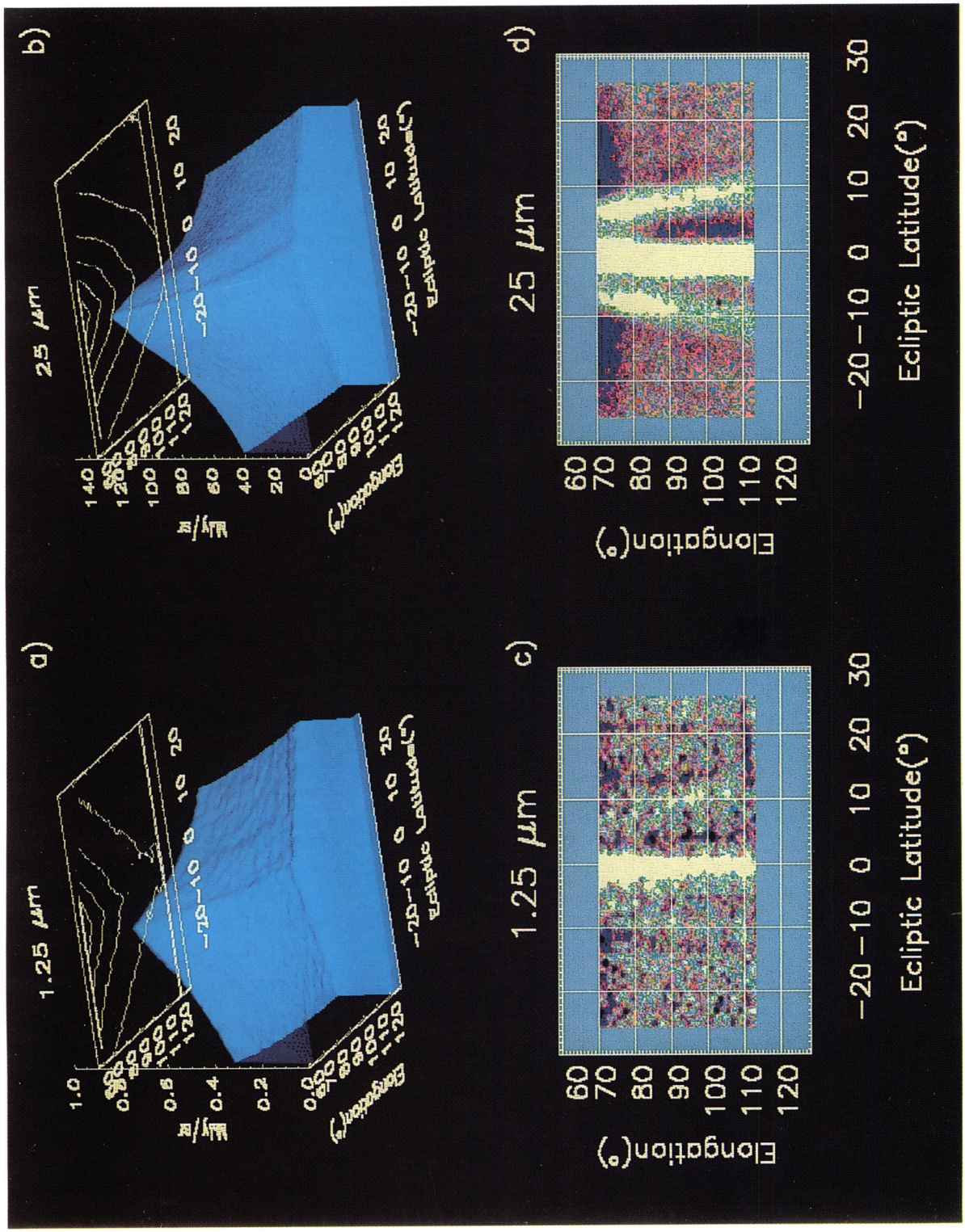

FIG. 1.—DIRBE images of dust near the ecliptic plane. (*a*) Surface plot of the 1.25 μm data. The peak of the smooth IPD is clearly evident as a ridge which rises toward the Sun. (*b*) Same as Fig. 1*a*, but for 25 μm data. Secondary ridges from the IPD band emission are visible. (*c*) Unsharp mask image of the data in Fig. 1*a* tuned to enhance the 10° bands, which appear to either side of the strong emission at the ecliptic plane. (*d*) Same as Fig. 1*c*, but for 25 μm data. Asymmetry between the northern and southern bands can be seen; the southern band becomes diffuse at the larger elongations.

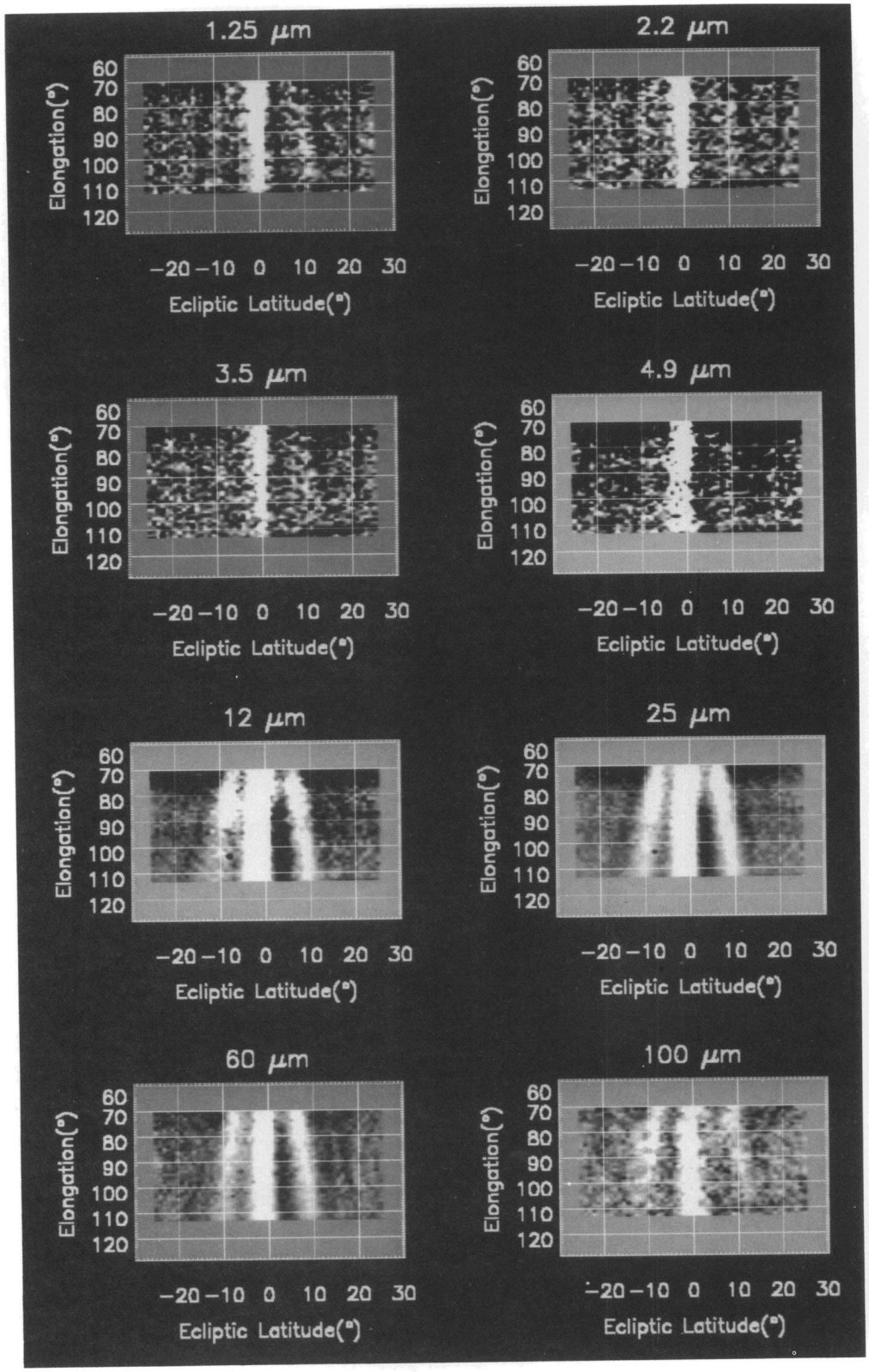

FIG. 2.—Unsharp mask intensity maps of the IPD bands from 1.25 to 100 μm

SPIESMAN et al. (see 442, 664)

Using equation (4) of Reach (1992),

$$\Delta \tan \beta \equiv (\tan \beta_N - \tan \beta_S) = \frac{2z}{\cos \epsilon + \sqrt{R^2 - \sin^2 \epsilon}} \quad (2)$$

where

β_N and β_S = the geocentric latitude of the northern and southern bands,
$2z$ = the distance between the bands in AU,
ϵ = solar elongation,
R = Sun centered band radius in AU ,

one finds heliocentric radii for the peak brightness of the $\pm 10°$ band of 2.05 ± 0.13 AU. We give weight only to the 1.25, 12, 25, 60, and 100 μm solutions, since precise identification of the band locations with elongation in the remaining (low S/N) images is difficult and leads to large systematic errors in the distance determination. For the $\pm 1\overset{\circ}{.}4$ bands, one finds heliocentric radii of 1.37 ± 0.17 AU. Results for all the wavelengths are shown in Table 2. The errors cited represent the range of band radii determinations found at different elongations. The $\pm 1\overset{\circ}{.}4$ bands are seen only at four wavelengths where the IPD signal is particularly strong because the DIRBE angular resolution is so close to the separation of these bands. The parallactic results are in excellent agreement with the results from *IRAS* data as shown in Table 3.

Although the "multiple exposure" technique for isolating the zodiacal emission blends features along the bands, there is still some fine structure in these images as seen in the northern and southern bands in Figure 1*d*. These local features along the bands are not accounted for in the simple model presented here, nor are they constrained by models found elsewhere in the literature.

TABLE 2

PARALLACTIC BAND RADII FOR THE INTERPLANETARY DUST BANDS BY WAVELENGTH

	10° BANDS		1°.4 BANDS	
WAVELENGTH (μm)	R	σ	R	σ
1.25	2.20	0.19	1.33	0.16
2.2	2.33	0.52		
3.5	2.17	0.18		
4.9	2.36	0.16		
12	1.99	0.08	1.45	0.13
25	1.88	0.12	1.32	0.08
60	2.16	0.08	1.36	0.29
100	2.04	0.20		
Weighted average	2.05	0.13	1.37	0.17

TABLE 3

COMPARISON OF DIRBE AND *IRAS* RESULTS

Parameter	DIRBE	*IRAS*
10° Bands		
$T_{thermal}$ (K)	185 ± 10	165–200[a]
$\tau_{thermal}$	1.01×10^{-8}	$\sim 10^{-8}$ [a]
$R_{thermal}$ (AU)	1.99 ± 0.2	2.2–3.2[a]
$R_{parallax}$ (AU)	2.05 ± 0.13	1.9 ± 0.2[b]
1°.4 Bands		
$R_{parallax}$ (AU)	1.37 ± 0.17	1.32 ± 0.05[b]

[a] Low et al. 1984.
[b] Reach 1992.

5.2. *Spectral Energy Distribution of the Bands*

The energy distributions of the IPD cloud and dust bands are fitted with gray body contributions from thermal emission and from scattered light (see Figs. 3 and 4). We estimate a 20% uncertainty for the intensity at each wavelength, which is dominated by the extraction of a rather weak signal. Thermal emission from the smooth component of the IPD cloud at $\beta = 0°$ can be fit to a dilute blackbody spectrum of 259 ± 10 K and an optical depth of 1.64×10^{-7}. The thermal emission from the $\beta = +10°$ band is consistent with a dilute black body spectrum with $T = 185 \pm 10$ K and an optical depth of 1.01×10^{-8}. This is 6.2% of the total optical depth at the ecliptic plane. The $1\overset{\circ}{.}4$ bands are too weak, too contaminated by the peak of the smooth IPD component, and too close together relative to the DIRBE angular resolution, even at the largest elongation angles observed, for a thermal analysis.

The scattered light from the smooth component of the dust cloud is roughly consistent with solar color and an optical depth of 3.16×10^{-8}, although Berriman et al. (1994) using DIRBE data find, and we confirm, that in the near infrared the IPD is slightly redder in color than is the Sun. This small color difference, which may be a signature of grain composition, has little effect on our analysis. The scattered light contribution from the $+10°$ dust band is similarly consistent with solar color, with optical depth 1.93×10^{-9}. This is 6.1% of the total optical depth at the ecliptic plane, very nearly the same ratio found for the thermal optical depths, implying similar optical properties between the smooth IPD and the band dust.

The color temperature of the thermal emission from the $+10°$ band can be used to find a heliocentric thermal band distance as is shown in equation (3),

$$R(\mathrm{AU}) = \left(\frac{278.29}{T}\right)^2 \sqrt{1 - A}\,, \quad (3)$$

where R is the heliocentric band distance measured in AU, T is the band particle temperature, and A is the scattering albedo of the band particles. The band temperature is consistent with that of a particle located at 1.99 ± 0.2 AU from the Sun. This value is reasonably consistent with the distance implied by the parallax analysis (Table 2) considering the fact that the bands may actually extend over an AU radially (Reach 1992). The color temperature of the smooth IPD cloud implies a similarly defined average heliocentric distance of 0.97 AU.

Assuming isotropic scattering, the apparent scattering albedo (determined at $\epsilon = 90°$) is given by

$$A_{90} = \frac{\tau_{sca}(90)}{\tau_{sca}(90) + \tau_{abs}}\,, \quad (4)$$

where τ_{sca} and τ_{abs} are, respectively, the scattering and thermal optical depths. Thus, $A_{90} = 0.13$ and 0.18 for the $+10°$ band and the IPD cloud, respectively. Using the normalized scattering phase function Φ derived from the angular variation of the zodiacal light (see Hong 1985; Lamy & Perrin 1986), the scattering albedo

$$A = \frac{A_{90}}{4\pi\Phi_{90}(1 - A_{90}) + A_{90}}\,, \quad (5)$$

so the albedo of the $+10°$ band and the IPD cloud are $A = 0.22$ and $A = 0.29$, respectively. The results of the energy distribution analyses appear in Table 4.

The IPD energy distributions were compared with Mie-theory spectra assuming spherical particles. Good fits were

TABLE 4

SUMMARY OF SPECTRAL RESULTS

IPD Region	$T_{thermal}$ (K)	$\tau_{thermal}$	$\tau_{scattering}$[a]	Albedo[b]
+10° band	185 ± 10	1.01×10^{-8}	1.93×10^{-9}	0.22
IPD cloud at $\beta = 0°$.....	259 ± 10	1.64×10^{-7}	3.16×10^{-8}	0.29

[a] Assuming $T_{\odot} = 5770$ K.

[b] Average of the albedos calculated using the phase functions of Hong 1985 and Lamy & Perrin 1986 separately.

found for solid particles composed of silicates and amorphous carbon with the IPD mass distribution of Grün et al. (1985). The model results indicate that the IPD is best characterized as silicate grains with less than 10% carbon content by weight, primarily because the addition of more amorphous carbon causes the particles to scatter too much solar radiation at 4.9 μm. In contrast, DIRBE observations of comets Austin, Levy, and Okazaki-Levy-Rudenko show that cometary grains require as much as 50% carbon content (Lisse et al. 1994; Lisse 1992). The model results imply that the total particle mass of the 10° band pair is 5×10^{13} kg (±50%), the mass of a typical small asteroid.

The origin of the IPD band grains, and perhaps much of the IPD cloud, is suggested to be asteroidal (Sykes et al. 1988; Dermott et al. 1994, 1995). The solid silicate particles inferred from the DIRBE energy distributions and the above models are consistent with the suggested IPD band grain origin in asteroidal debris. Polarization analysis of the IPD also indicates that the smooth IPD particles are solid (Berriman et al. 1994). In contrast, Lisse et al. (1994) found cometary grains to be porous with a different, larger size distribution, using the same modeling techniques as employed here.

A comparison of albedos also shows differences between cometary dust and IPD particles. The IPD particles are more reflective than dust in comet tails; the albedo of comet Austin dust is 0.065, and that of the particularly reflective comet Levy dust is 0.13, although its high albedo is caused by an excess of small particles (Lisse 1992). Even when corrected using an appropriate comet-based phase function (Grün & Jessberger 1990), the cometary albedos are less than IPD albedos (Table 4). This could result from the larger grain size of the comet dust, but modeling results indicate that it is, instead, a result of darker material in comets. Since comet nuclei are darker ($A = 0.03$ to 0.05 for Halley; Grün & Jessberger 1990) than most Earth approaching asteroids ($A = 0.1$ to 0.3; Clark et al. 1992), the difference in grain albedo might indicate a real chemical or mineral composition difference between the likely progenitors of the grains. The fact that both the IPD and the most numerous near-Earth asteroids, the S-Type asteroids, are redder than the Sun at near infrared wavelengths (Johnson et al. 1975; Clark et al. 1992) furthers the hypothesis of asteroidal grain origin, although there is a hint that comet dust may also be redder than solar (Lisse et al. 1994).

One other point to note is that the band grains are darker than the IPD grains of the smooth cloud, suggesting that the IPD band particles may be larger than the particles that produce the smooth IPD cloud emission. This can be understood in the context of asteroidal debris being the source of IPD grains. After an asteroidal disruption, grains differentially migrate out of their original orbits, which coincide with the IPD bands, and into the smooth IPD as a result of Poynting-Robertson drag. The larger size, lower albedo particles remain in the bands longer. The rates of orbital decay range over more than an order of magnitude for the particles considered here (10^5 to 10^7 years; Reach 1992), so the darkening of the bands with time should be observable; one might even be able to relate the amount of darkening to the recent history of asteroidal disruptions, but this would be difficult because of the large uncertainty in the mineralogical composition of the progenitor and because older particles would tend to be further darkened by surface processing from long exposure to the solar wind.

5.3. *Band Morphology and Temporal Change*

Images of the dust bands have been prepared for various times during the 10 month long *COBE* cold mission. Although the multiple exposure imaging technique smears out small discrete features, DIRBE observes subtle local changes in band width and separation through the mission as did *IRAS* (Sykes 1990). Because DIRBE scans only a portion of the bands at any given time, it is difficult to separate spatial from temporal band changes. Since the DIRBE does map two pieces of the bands at a given time, one looking forward in the Earth's orbit and one looking backward, it is possible to make sets of full orbit images (offset in time by $\frac{1}{4}$ of a year) in order to differentiate between temporal and spatial band variations. Though results of such an analysis are not yet available, the *IRAS* and DIRBE data combined provide a 7 year baseline of dust band data, and there is no evidence for gross changes in the band systems between the two missions. The more subtle apparent changes in the bands during the *COBE* mission most reasonably can be attributed to real variations in band density with location and/or time.

6. CONCLUSIONS

DIRBE data confirm the *IRAS* observations of emission from the interplanetary dust bands at 12, 25, 60, and 100 μm, and provide the first observational evidence of the dust bands in scattered solar light. The scattered light observations offer important new clues as to the composition and origin of the bands and the smooth IPD cloud. We find that the spectral properties and inferred composition of the IPD band grains, as well as those in the smooth IPD cloud, are different than those found in cometary grains. We conclude that the IPD bands and the smooth IPD cloud are heavily populated by grains of asteroidal origin.

The authors gratefully acknowledge the many colleagues who contributed to the success of the *COBE* mission. We are particularly appreciative of the prodigious efforts of the staff of the Cosmology Data Analysis Center, and especially those of the DIRBE data teams lead by J. A. Skard and G. Toller, for producing the high quality data sets used in this work. One of us (W. J. S.) would like to thank Richard White for suggesting that a study of the dust bands be undertaken.

REFERENCES

Berriman, G. B., et al. 1994, ApJ, 431, L63
Boggess, N. W., et al. 1992, ApJ, 397, 420
Clark, B. E., et al. 1992, Icarus, 97, 288
Dermott, S. F., et al. 1984, Nature, 312, 505
———. 1988, in Comets to Cosmology, ed. A. Lawrence (London: Springer), 3
———. 1994, Nature, 369, 719
———. 1995, in IAU Symp. 160, Asteroids, Comets and Meteors, in press
Grün, E., & Jessberger, E. K. 1990, in Physics and Chemistry of Comets, ed. W. F. Huebner (Berlin: Springer), 113
Grün, E., et al. 1985, Icarus, 62, 244
Hauser, M. G. 1993, in AIP Conf. Proc. 278: Back to the Galaxy, ed. S. S. Holt & F. Verter (New York: AIP), 201
Hauser, M. G., et al. 1984, ApJ, 278, L19
———. 1991, in AIP Conf. Proc. 222: After the First Three Minutes, ed. S. S. Holt, C. Bennett, & V. Trimble (New York: AIP), 161
Hong, S. S. 1985, A&A, 146, 67
Johnson, T. V., et al. 1975, ApJ, 197, 527
Lamy, P. L., & Perrin, J.-M. 1986, A&A, 163, 269
Lisse, C. M. 1992, Ph.D. thesis, Univ. Maryland
Lisse, C. M., et al. 1994, ApJ, 432, L71
Low, F. J., et al. 1984, ApJ, 278, L19
Reach, W. T. 1991a, in Origin and Evolution of Interplanetary Dust, ed. A. C. Levasseur-Regourd & H. Hasegawa (Tokyo: Kluwer), 211
———. 1991b, ApJ, 369, 529
———. 1992, ApJ, 392, 289
Silverberg, R. F., et al. 1993, in Proc. SPIE 2019, 180
Sykes, M. V. 1988, ApJ, 334, L55
———. 1990, Icarus, 84, 267
Sykes, M. V., et al. 1988, in Asteroids II, ed. R. P. Binzel, T. Gehrels, & M. Mathews (Tucson: Univ. Arizona Press), 336
Sykes, M. V., & Greenberg, R. 1986, Icarus, 65, 51